Original Article | Breast Imaging

eISSN 2005-8330
https://doi.org/10.3348/kjr.2020.0310
Korean J Radiol 2021;22(4):502-512

Korean Journal of Radiology
KJR

Subjective and Objective Assessment of Monoenergetic and Polyenergetic Images Acquired by Dual-Energy CT in Breast Cancer

Xiaoxia Wang, MD*, Daihong Liu, PhD*, Shixi Jiang, MD, Xiangfei Zeng, MD, Lan Li, MD, Tao Yu, MD, Jiuquan Zhang, PhD

All authors: Department of Radiology, Chongqing University Cancer Hospital & Chongqing Cancer Institute & Chongqing Cancer Hospital, Chongqing, China

Objective: To objectively and subjectively assess and compare the characteristics of monoenergetic images [MEI (+)] and polyenergetic images (PEI) acquired by dual-energy CT (DECT) of patients with breast cancer.

Materials and Methods: This retrospective study evaluated the images and data of 42 patients with breast cancer who had undergone dual-phase contrast-enhanced DECT from June to September 2019. One standard PEI, five MEI (+) in 10-kiloelectron volt (keV) intervals (range, 40–80 keV), iodine density (ID) maps, iodine overlay images, and Z effective (Z_{eff}) maps were reconstructed. The contrast-to-noise ratio (CNR) and the signal-to-noise ratio (SNR) were calculated. Multiple quantitative parameters of the malignant breast lesions were compared between the arterial and the venous phase images. Two readers independently assessed lesion conspicuity and performed a morphology analysis.

Results: Low keV MEI (+) at 40–50 keV showed increased CNR and $SNR_{breast\ lesion}$ compared with PEI, especially in the venous phase ([CNR: 40 keV, 20.10; 50 keV, 14.45; vs. PEI, 7.27; $p < 0.001$], [$SNR_{breast\ lesion}$: 40 keV, 21.01; 50 keV, 16.28; vs. PEI, 10.77; $p < 0.001$]). Multiple quantitative DECT parameters of malignant breast lesions were higher in the venous phase images than in the arterial phase images ($p < 0.001$). MEI (+) at 40 keV, ID, and Z_{eff} reconstructions yielded the highest Likert scores for lesion conspicuity. The conspicuity of the mass margin and the visual enhancement were significantly better in 40-keV MEI (+) than in the PEI ($p = 0.022$, $p = 0.033$, respectively).

Conclusion: Compared with PEI, MEI (+) reconstructions at low keV in the venous phase acquired by DECT improved the objective and subjective assessment of lesion conspicuity in patients with malignant breast lesions. MEI (+) reconstruction acquired by DECT may be helpful for the preoperative evaluation of breast cancer.

Keywords: *Dual-energy computed tomography; Monoenergetic images; Polyenergetic images; Breast cancer; Quantitative parameters*

INTRODUCTION

Breast cancer is the most frequently diagnosed cancer among women and is also the leading cause of cancer-related death in over 100 countries (1). Routine diagnostic imaging of breast cancer includes mammography,

Received: January 14, 2020 **Revised:** September 4, 2020 **Accepted:** September 27, 2020
This study has received funding by the National Natural Science Foundation of China (Grant No. 82071883), the combination projects of medicine and engineering of the Fundamental Research Funds for the Central Universities in 2019 (Project No. 2019CDYGYB008), the Chongqing key medical research project of combination of science and medicine (Grant No. 2019ZDXM007), and the 2019 SKY Imaging Research Fund of the Chinese International Medical Foundation (Project No. Z-2014-07-1912-10).
*These authors contributed equally to this work.
Corresponding author: Jiuquan Zhang, PhD, Department of Radiology, Chongqing University Cancer Hospital & Chongqing Cancer Institute & Chongqing Cancer Hospital, No.181 Hanyu Road, Shapingba District, Chongqing 400030, China.
• E-mail: zhangjq_radiol@foxmail.com

Korean Journal of Radiology
KJR

ultrasonography (US), and MRI (2, 3). MRI, with its high soft tissue resolution, is a commonly used method for a multi-parametric, multi-azimuthal, and multi-sequence examination of breast cancer. However, high cost and limited accessibility are obstacles to its use for breast cancer examination.

Chest CT, used for the evaluation of potential lung metastasis or concomitant pulmonary disease (4), is unable to precisely characterize primary breast tumors (5) because of its relatively low soft tissue resolution. Recently, a noise-optimized virtual monoenergetic image reconstruction algorithm [MEI (+)] was developed, which has been shown to improve the signal-to-noise ratio (SNR) and the contrast-to-noise ratio (CNR) in oncological imaging (6-8). Although dual-energy CT (DECT) has proven feasibility in the imaging of primary breast cancers (9), the use of more reconstruction images, such as iodine density (ID) maps (10), iodine overlay (IO) images, and Z effective (Z_{eff}) maps (11), as well as polyenergetic images (PEI) should be considered when investigating lesion conspicuity.

In addition, quantitative parameters can be obtained from DECT, namely the normalized iodine concentration (NIC), the slope of the spectral Hounsfield unit (HU) curve (λ_{HU}, HU per kiloelectron volt [keV]), and the normalized effective atomic number (nZ_{eff}). These quantitative parameters are useful for tumor detection, lesion characterization, and assessment of treatment response (12-14). The few studies that have used individual quantitative parameters have shown that the iodine concentration is significantly higher in tumors than in normal breast tissue and pectoral muscle (9). However, the characteristics of DECT quantitative parameters in dual-phase scans of malignant breast lesions have not been studied.

The purpose of this study was to objectively and subjectively assess the image characteristics of MEI (+) and PEI acquired by DECT in patients with breast cancer. Image characteristics were the primary outcome of this study, and the characteristics of the quantitative parameters of dual-phase DECT and morphological analysis were the secondary outcomes.

MATERIALS AND METHODS

Patients Characteristics

This single-center study was approved by the ethics committee of our hospital (IRB No. CZLS20200215-A). The need for written informed consent was waived because of the retrospective study design. From June to September 2019, 75 patients with high suspicion of breast cancer on mammography, US, and/or MRI (Breast Imaging-Reporting and Data System category 4C/5, 28 patients), or those with a pathological diagnosis of breast cancer (47 patients) underwent dual-phase contrast-enhanced DECT for the evaluation of potential lung metastasis or concomitant pulmonary disease. The included patients were women with a primary diagnosis of breast cancer with pathological confirmation and who were not pregnant. The exclusion criteria were as follows: mass biopsy within one week before CT scanning (n = 10), neoadjuvant chemotherapy before CT scanning (n = 16), absence of complete pathological information (n = 3), or breast mass exceeding the field of view because of obesity (n = 4). Finally, 33 patients were excluded, and the remaining 42 patients with breast cancer, confirmed by histopathology of US-guided core needle biopsy specimens, were included.

The immunohistochemical results of estrogen receptor (ER), progesterone receptor (PR), human epidermal growth factor receptor 2 (HER2), and Ki-67 were classified as positive or negative (15). ER and PR positivity were defined as ≥ 1% of nuclear immunostaining. HER2 was considered positive when the immunohistochemistry staining intensity score was ≥ 3. An immunohistochemistry HER2 score of 2+ was further explored by gene amplification with fluorescence *in situ* hybridization. Ki-67 was assessed as the percentage of immunoreactive tumor cells, and a cutoff value of 20% was used to define the positive and negative groups (16).

DECT Image Acquisition

Image data were acquired on a 2.5 generation dual-source CT unit (SOMATOM Drive, Siemens Healthineers) in dual-energy mode through two X-ray tubes with different kV tube voltages (tube A, 100 kV; tube B, Sn 140 kV), using a tin filter for the high-voltage tube. Automatic exposure control (CARE Dose 4D, Siemens Healthineers) was used in all scans. The settings for the scanners were as follows: collimation, 64 x 0.6 mm; rotation time, 0.28 seconds; pitch, 0.55; reference tube current time product, 71 mAs for the 100 kV tube and 60 mAs for the Sn 140 kV tube; reformatted section thickness, 1.5 mm; reformatted section increment, 1.5 mm.

All patients were scanned craniocaudally in supine position. Non-contrast DECT images were acquired first. For contrast-enhanced scanning, iodinated nonionic

 https://doi.org/10.3348/kjr.2020.0310

contrast media (ioversol, 320 mgI/mL, Hengrui Medicine) was administered through the ulnar vein at a dose of 1.5 mL/kg with a flow rate of 2.5 mL/s, followed by a bolus injection of 30 mL of saline at the same flow rate. After the injections, the arterial phase scans were started using a bolus-tracking technique with a threshold of 100 HU in the descending aorta and an additional delay of 10 seconds (average, 35 ± 5 seconds). The scan delay time for the venous phase scanning was 25 seconds after the end of the arterial phase scanning (average, 60 ± 7 seconds).

DECT Image Reconstruction

Reconstructed CT image data were post-processed on a syngo.via workstation (VB20A, Dual Energy, Siemens Healthineers). Standard linear-blended images (that is, PEI) were reconstructed by applying a blending factor of 0.5 (M_0.5; 50% of the low kV and 50% of the high kV spectrum). MEI (+) was reconstructed at 40, 50, 60, 70, and 80 keV levels, as well as ID and Z_{eff} series and IO images. No reconstructions at higher keV levels were performed, as previous studies have suggested that optimal keV levels range from 40 to 70 keV (9, 17). ID images are material-specific images calculated from two different energetic datasets (100% iodine concentration); when fused with regular grayscale conventional images, leading to IO images, the iodine concentration appears color-coded (50% iodine concentration). Z_{eff} maps display the atomic numbers of the scan volume in a color-coded manner.

Objective Image Analysis

Quantitative analysis was performed by two experienced radiologists (with 7 years of experience in breast and chest diagnostic imaging, and with 2 years of experience in post-reconstruction imaging), who placed circular regions of interest (ROI) with constant sizes of 1 cm^2 (only adjusted to prevent the inclusion of tissues of different attenuations) (18), excluding any area of obvious gross necrosis, calcification, or large vessels, within the following predefined regions: breast lesion, ipsilateral pectoral muscle, and normal fibroglandular breast tissue. Three measurements of HU and standard deviation (SD) were conducted on PEI and on 40–80 keV MEI (+), and average values were recorded. CNR and SNR were calculated according to the following formulas:

$$CNR = (HU_{\text{breast lesion}} - HU_{\text{normal fibroglandular breast tissue}})/SD_{\text{(air)}}$$

$$SNR_{\text{breast lesion}} = HU_{(\text{breast lesion})}/SD_{\text{(air)}}$$

$$SNR_{\text{ipsilateral pectoral muscle}} = HU_{(\text{ipsilateral pectoral muscle})}/SD_{\text{(air)}}$$

$$SNR_{\text{normal fibroglandular breast tissue}} = HU_{(\text{normal fibroglandular breast tissue})}/SD_{\text{(air)}}$$

Dual-energy quantitative parameters were measured by placing a ROI in the breast lesions in the arterial and venous phases. Quantitative parameters, including the iodine concentration and the effective atomic number, were divided by the iodine concentration and the effective atomic number of the aorta, respectively, to obtain the NIC and the nZ_{eff}. The λ_{HU} was defined as the difference between the CT value at 40 keV and that at 70 keV divided by the energy difference (30 keV), and it was calculated as follows:

$$\lambda_{HU} = (HU_{40\ keV} - HU_{70\ keV})/30\ keV \quad (19)$$

Subjective Image Analysis

To assess breast lesions subjectively, two experienced radiologists (with 7 years of experience, and with 27 years of experience in breast and chest diagnostic imaging) reviewed the PEI, the MEI (+) at 40–80 keV levels, and the ID, IO, and Z_{eff} reconstructions, and evaluated lesion conspicuity by using a five-point Likert scale (1: barely perceived; 2: subtly visualized; 3: fairly detectable; 4: definitely detected; 5: strikingly evident/easily spotted) (17). They were informed about the presence of breast cancer in all patients but were blinded to the image reconstruction method.

Morphological analysis was performed for the optimal MEI (+) and PEI groups. Due to the lack of a formal lexicon for breast CT imaging, a consensus analysis of morphology was achieved by using the Breast Imaging-Reporting and Data System lexicons of MRI-detected breast lesions as the reference (20, 21). The DECT characteristics of each lesion were analyzed as follows: lesion type (mass or non-mass), shape (oval, round, lobulated, or irregular), and margin (circumscribed or non-circumscribed; in the case of mass lesions). Visual enhancement was evaluated for all lesion types as 'poor' or 'good' (20), where 'good' indicated a more conspicuous lesion on enhanced CT images than on the unenhanced CT images; otherwise, visual enhancement was described as 'poor'.

Statistical Analysis

Statistical analyses were performed using statistical software (IBM SPSS Statistics, version 22.0; IBM Corp.). To assess inter-observer agreement in the quantitative analysis, we used the intraclass correlation coefficient (ICC)

https://doi.org/10.3348/kjr.2020.0310

Korean Journal of Radiology
KJR

with a two-way random model of consistency. Inter-observer agreement for the Likert scale was calculated using Cohen's kappa coefficients. To compare quantitative parameters of DECT between the arterial and the venous phase, the Mann-Whitney U-test and the two-sample *t* test were used. To compare CNR, SNR, and lesion conspicuity scores, one-way analysis of variance (ANOVA) with Tukey's post hoc test and the non-parametric Kruskal-Wallis H test were used. Pairwise comparisons with Bonferroni correction were performed to assess significant results. Morphological analysis was conducted using the χ^2 test. The level of significance was set at $p < 0.05$.

RESULTS

Patients Characteristics

Finally, 42 pathologically proven breast cancers were analyzed as representative lesions in 42 patients (average age, 54.6 ± 11.7 years). The average maximal tumor diameter was 2.67 ± 0.89 cm. Histopathologically, 25 lesions were invasive ductal carcinoma, 9 were lobular invasive carcinoma, 5 were ductal carcinoma *in situ*, 2 were mucinous carcinoma, and one lesion was a medullary carcinoma. Patient demographics and histopathological characteristics are described in Table 1.

The mean cumulative CT dose was 5.44 ± 1.92 mGy, and the mean dose length product was 165.32 ± 55.34 mGy x cm. The average effective dose was 2.3 ± 0.77 mSv for each phase.

Table 1. Patient Demographics and Histopathological Characteristics of 42 Patients with Breast Cancers

Characteristics	Number
Age, mean ± SD, years (range)	54.6 ± 11.7 (36–87)
The maximal tumor diameter, mean ± SD, cm (range)	2.67 ± 0.89 (1.1–7.2)
T category (%)	
Tis	5 (11.9)
T1	10 (23.8)
T2	18 (42.8)
T3	2 (4.7)
T4	7 (16.8)
Menstruation state (%)	
Premenopausal women	12 (28.6)
Postmenopausal women	24 (57.2)
Perimenopausal women	6 (14.2)
Histologic type of malignant lesions (%)	
Invasive ductal carcinoma	25 (59.5)
Invasive lobular carcinoma	9 (21.4)
Ductal carcinoma *in situ*	5 (11.9)
Mucinous carcinoma	2 (4.8)
Medullary carcinoma	1 (2.4)
Estrogen receptor status (%)	
Positive	25 (59.5)
Negative	17 (40.5)
Progesterone receptor status (%)	
Positive	16 (38.1)
Negative	26 (61.9)
Human epidermal growth factor receptor 2 status (%)	
Positive	10 (23.8)
Negative	32 (76.2)
Ki-67 status (%)	
Positive	33 (78.6)
Negative	9 (21.4)

SD = standard deviation

Objective Image Quality Parameters

The quantitative SNR and CNR values are detailed in Table 2 and illustrated in Figure 1. MEI (+) at 40 keV and at 50 keV provided the highest CNR in both the arterial (40 keV CNR, 14.05; 50 keV CNR, 10.07) and the venous phase (40 keV CNR, 20.10; 50 keV CNR, 14.45). The abovementioned values were significantly higher than the CNR of PEI and of MEI (+) at 60–80 keV (adjusted *p* range, < 0.001–0.048). The $SNR_{breast\ lesion}$ showed the highest values at 40–50 keV MEI (+) ([arterial phase: 40 keV, 16.62; 50 keV, 13.51], [venous phase: 40 keV, 21.01; 50 keV, 16.28]), and they were significantly higher than the $SNR_{breast\ lesion}$ of PEI and of MEI (+) at 60–80 keV (adjusted *p* range, < 0.001–0.040). The $SNR_{ipsilateral\ pectoral\ muscle}$ at 40 keV MEI (+) (arterial phase, 11.99; venous phase, 12.82) was significantly higher than that of PEI (adjusted *p* range, 0.030–0.035). For the $SNR_{normal\ fibroglandular\ breast\ tissue}$, there was no statistically significant difference between MEI (+) and PEI. The ICCs for inter-observer variability in terms of quantitative parameters were 0.937 (0.761–0.989) for the arterial phase and 0.918 (0.751–0.990) for the venous phase.

The comparison of multiple quantitative DECT parameters between the arterial and the venous phase in malignant breast lesions is summarized in Table 3. The venous phase NIC, nZ_{eff}, and λ_{HU} were significantly higher than those in the arterial phase (all $p < 0.001$). Representative images are shown in Figure 2.

Subjective Image Analysis

A summary of lesion conspicuity scores is presented in

https://doi.org/10.3348/kjr.2020.0310

Table 2. Quantitative Values for CNR and SNR in the Arterial and Venous Phase

	PEI	40 keV MEI (+)	50 keV MEI (+)	60 keV MEI (+)	70 keV MEI (+)	80 keV MEI (+)	*P*
Arterial phase							
CNR	5.73 (2.73, 8.73)	14.05 (8.53, 18.99)	10.07 (5.50, 14.94)	9.25 ± 7.23	7.62 (4.50, 11.0)	6.58 (3.44, 10.77)	< 0.001*
$SNR_{breast\ lesion}$	9.39 ± 4.23	16.62 (10.34, 21.72)	13.51 (8.07, 17.24)	11.71 ± 6.31	10.22 ± 5.08	9.15 ± 4.55	< 0.001
$SNR_{ipsilateral\ pectoral\ muscle}$	9.06 ± 3.63	11.99 ± 6.50	10.49 ± 4.85	9.80 ± 4.13	9.31 ± 3.71	8.78 ± 3.81	0.014†
$SNR_{fibroglandular\ breast\ tissue}$	2.89 ± 3.88	2.80 ± 3.12	2.67 ± 3.34	2.42 ± 3.61	1.96 ± 4.54	1.49 ± 5.99	0.366
Venous phase							
CNR	7.27 ± 4.94	20.10 ± 13.74	14.45 ± 9.63	10.68 ± 7.17	8.17 ± 5.56	6.70 ± 4.60	< 0.001
$SNR_{breast\ lesion}$	10.77 ± 4.48	21.01 (14.89, 28.55)	16.28 (11.71, 20.88)	12.80 (8.88, 16.08)	10.7 (7.65, 13.46)	9.40 (6.82, 11.71)	< 0.001
$SNR_{ipsilateral\ pectoral\ muscle}$	9.10 ± 3.13	12.82 ± 5.70	10.46 ± 4.76	9.99 ± 3.77	9.28 ± 3.48	8.50 ± 3.27	0.001
$SNR_{fibroglandular\ breast\ tissue}$	3.50 ± 3.25	3.74 ± 5.61	3.53 ± 2.78	3.51 ± 3.13	3.46 ± 4.32	3.21 ± 3.72	0.931

$p < 0.05$ indicate statistically significant. *The non-parametric with Kruskal-Wallis H Test for non-normally distributed data (median [QR]), †The one-way ANOVA with Tukey's post-hoc test for normally distributed continuous data (means ± SD). ANOVA = analysis of variance, CNR = contrast-to-noise ratio, keV = kiloelectron volt, MEI (+) = noise-optimized virtual monoenergetic images, PEI = polyenergetic images, QR = quartile range, SNR = signal-to-noise ratio

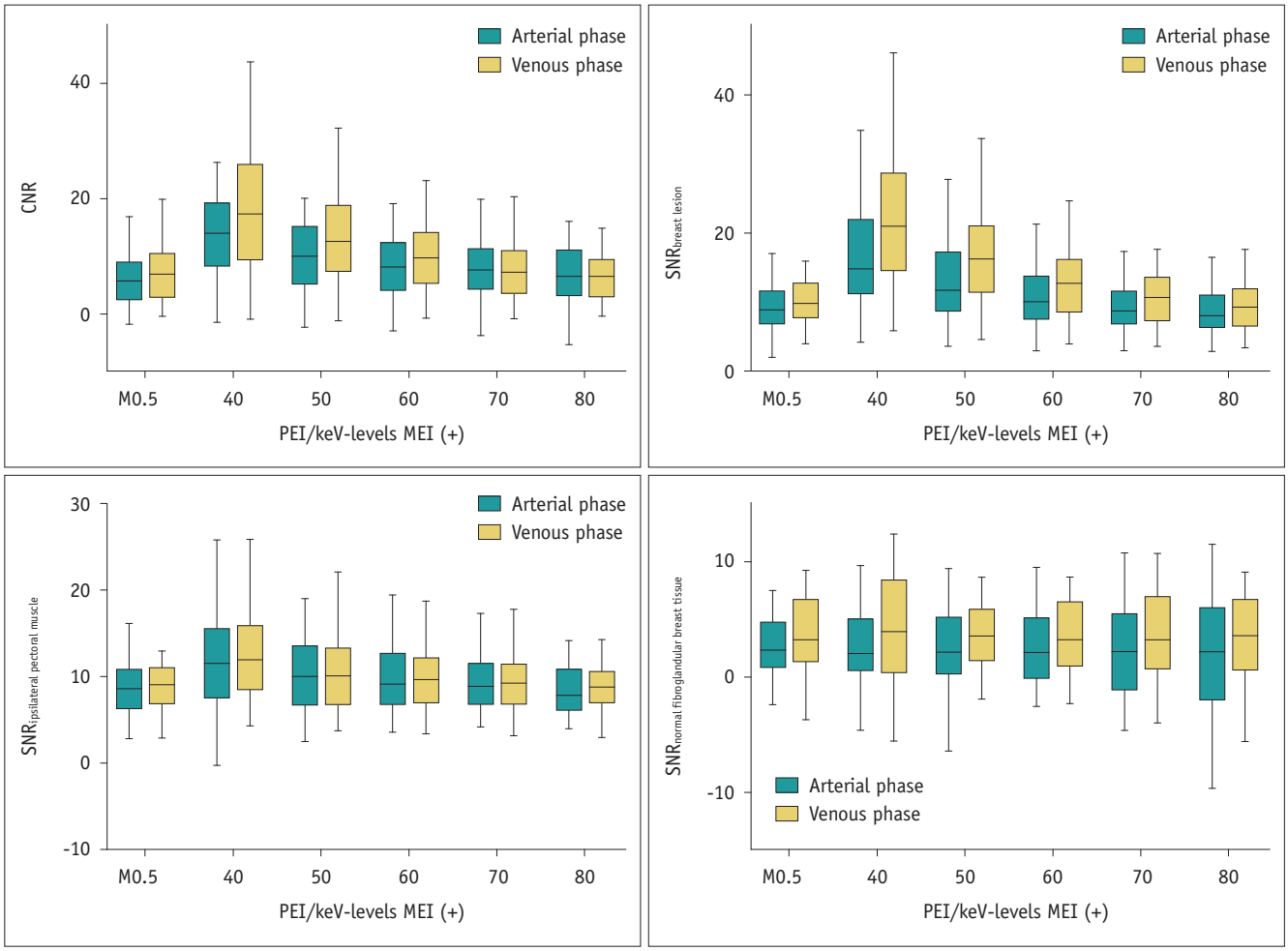

Fig. 1. Box-and-whisker plots of CNR and SNR for the PEI and MEI (+) reconstructions acquired at 40–80 keV. The boxes represent the middle 50% of the cases, the horizontal lines within the boxes, the median values, and the whiskers, the minimal and maximal values (n = 42). CNR = contrast-to-noise ratio, keV = kiloelectron volt, MEI (+) = noise-optimized virtual monoenergetic images, PEI = polyenergetic images, SNR = signal-to-noise ratio

https://doi.org/10.3348/kjr.2020.0310

Korean Journal of Radiology
KJR

Table 4. Lesion conspicuity scores were significantly higher at 40 keV MEI (+), ID, and Z_{eff} reconstructions than PEI and MEI (+) reconstruction acquired at 50–80 keV levels (adjusted $p < 0.001$). There was no statistically significant difference between the arterial and the venous phase images. Representative images are shown in Figure 3. For subjective image analysis, inter-observer agreement ranged between substantial and excellent, with kappa values of 0.735–0.940.

Based on the results of the objective image quality parameters and of the subjective evaluation, we selected the venous phase of 40 keV MEI (+) and of PEI for morphological analysis. A summary of the lesion morphological analysis is presented in Table 5. The conspicuity of the mass margin and the visual enhancement were significantly higher at 40 keV MEI (+) than at PEI (p = 0.022 and p = 0.033, respectively). Regarding greatest axial diameter, type, shape, and concomitant sign, there were no differences between 40 keV MEI (+) and PEI.

Table 3. Multiple Quantitative Parameters of Dual-Energy CT between Arterial Phase and Venous Phase in Breast Malignant Lesions

Quantitative Parameters	Arterial Phase	Venous Phase	t/Z Value	*P*
NIC	0.119 ± 0.071	0.363 (0.247, 0.449)	-9.762	< 0.001*
λ_{HU} (HU/keV)	1.85 ± 0.88	2.76 ± 1.15	-4.062	< 0.001†
nZ_{eff}	0.73 ± 0.04	0.87 (0.84, 0.91)	-15.865	< 0.001

$p < 0.05$ indicates statistical significance. *The Mann-Whitney U-test for non-normally distributed data (median [QR]), †Two sample *t* test for normally distributed continuous data (means ± SD). HU = Hounsfield unit, NIC = normalized iodine concentration, nZ_{eff} = normalized effective atomic number, λ_{HU} = slope of the spectral HU curve

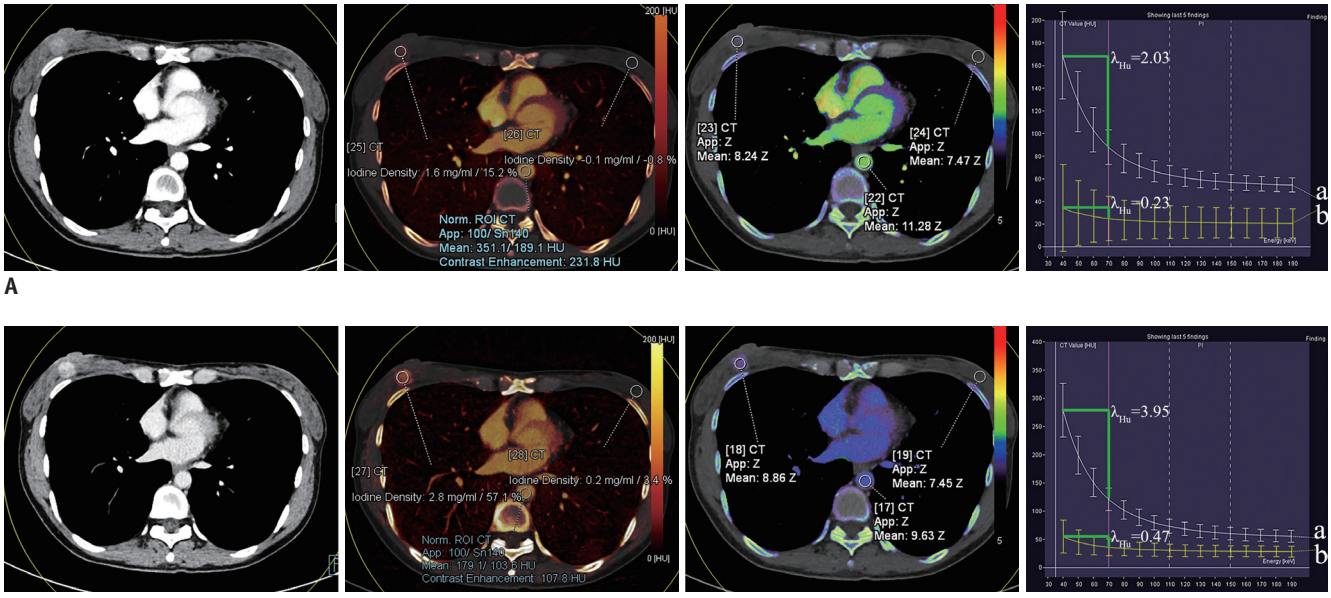

Fig. 2. Representative dual-energy CT images of a 44-year-old woman with right breast invasive ductal carcinoma.
(**A,** arterial phase; **B,** venous phase; PEI - pseudocolored image for iodine concentration - pseudocolored image for effective atomic number - graph for λ_{HU}, in order). HU = Hounsfield unit, ROI = regions of interest, λ_{HU} = slope of the spectral HU curve

Table 4. Lesion Conspicuity Scores in Arterial and Venous Phases

	PEI	40 keV MEI (+)	50 keV MEI (+)	60 keV MEI (+)	70 keV MEI (+)	80 keV MEI (+)	ID	IO	Z_{eff}	*P*
Arterial phase	3.10 ± 0.43	4.95 ± 0.22	4.12 ± 0.33	3.83 ± 0.38	3.20 ± 0.38	2.19 ± 0.51	4.93 ± 0.26	3.07 ± 0.46	4.93 ± 0.26	< 0.001
Venous phase	3.12 ± 0.45	4.95 ± 0.21	4.17 ± 0.37	3.88 ± 0.33	3.20 ± 0.39	2.28 ± 0.46	4.95 ± 0.22	3.10 ± 0.48	4.95 ± 0.22	< 0.001

$p < 0.05$ indicates statistical significance. *P* values are obtained from the comparisons among the 9 groups by one-way ANOVA test. ID = iodine density, IO = iodine overlay, Z_{eff} = Z effective

https://doi.org/10.3348/kjr.2020.0310

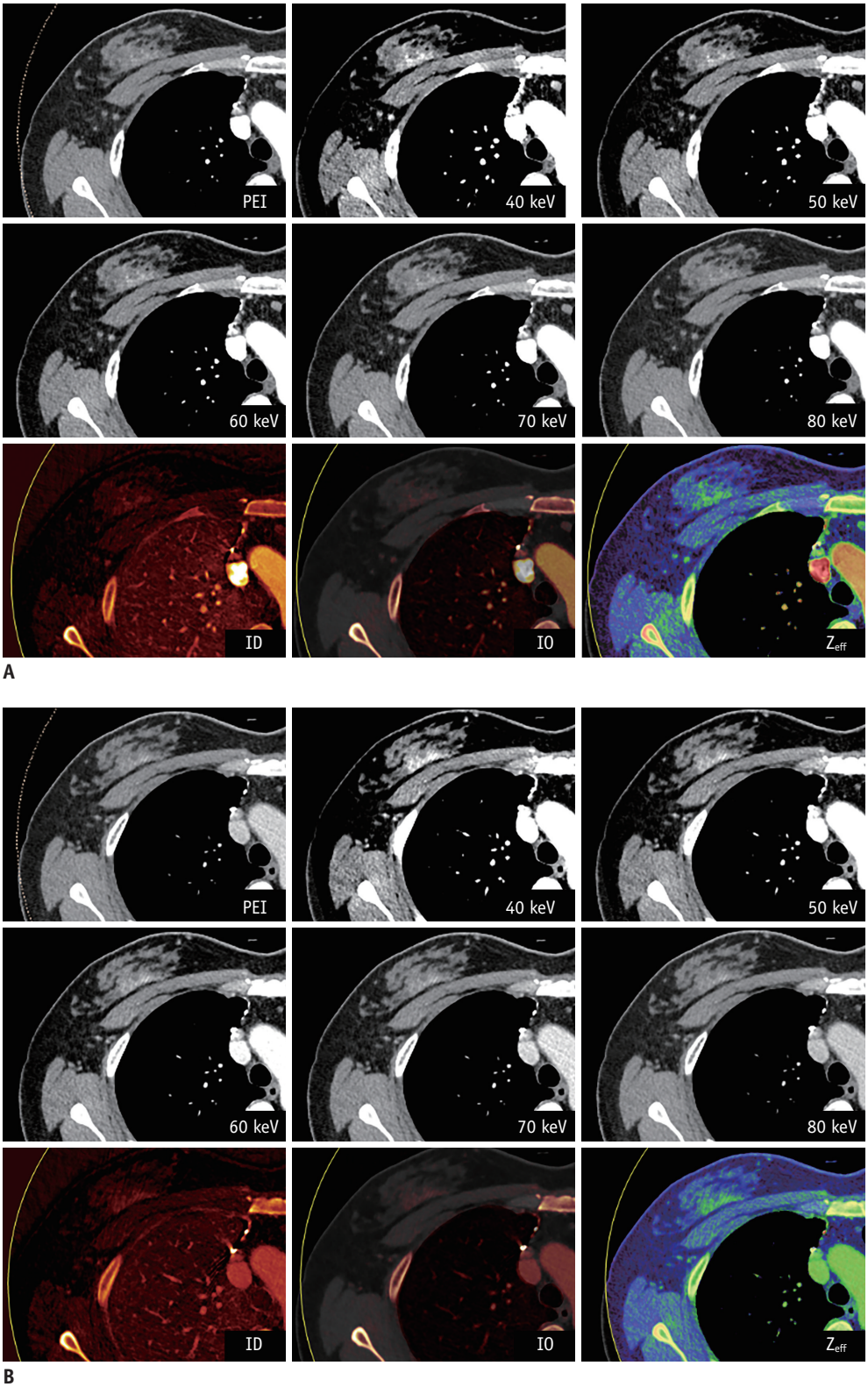

Fig. 3. Axial images of a 55-year-old man patient with right breast invasive ductal carcinoma (non-mass lesion).
A. Arterial phase. **B.** Venous phase. There is good visual enhancement of the lesions in 40 keV MEI (+), while there is poor visual enhancement of the lesions in PEI. ID = iodine density, IO = iodine overlay, Z_{eff} = Z effective

https://doi.org/10.3348/kjr.2020.0310

Korean Journal of Radiology
KJR

Table 5. Differences in Morphological Analysis between 40 keV MEI (+) and PEI of Venous Phase in 42 Breast Cancers

Parameters	40 keV MEI (+)	PEI	*t* Value/Chi-Squares	*P*
The maximal tumor diameter (cm)	2.75 ± 1.16	2.81 ± 1.20	-0.202	0.840*
Lesion type				
Mass	22	21	0.048	0.827†
Non-mass	20	21		
Mass shape				
Oval, round	10	9	0.029	0.864
Irregular, lobulated	12	12		
Mass margin				
Circumscribed	15	7	5.222	0.022
Non-circumscribed	7	14		
Visual enhancement pattern				
Poor	5	13	4.525	0.033
Good	37	29		
Concomitant sign				
Invasion of skin	7	7	< 0.001	1.000
Invasion of nipple	6	6	< 0.001	1.000
Invasion of muscle	2	2	< 0.001	1.000
Axillary node abnormality	55	55	NA	NA

$p < 0.05$ indicates statistical significance. *Two sample *t* test for normally distributed continuous data (means ± SD), †The χ^2 test for categorical variables. NA = not applicable

DISCUSSION

This study showed that compared with PEI, MEI (+) reconstructions at low keV acquired by DECT improved subjective and objective assessment of lesion conspicuity in patients with breast cancer. Our findings seem to indicate that MEI (+) reconstruction acquired by DECT may be useful for the preoperative evaluation of breast cancer.

Several studies in organs other than the breast have shown that MEI (+) reconstructions are superior to PEI, as they can provide excellent image quality by virtue of their significantly lower image noise at similar attenuation levels (6, 7). The MEI (+) technique performs recombination based on spatial frequency, which reduces the image noise at lower levels and improves the image contrast at higher energies to obtain the best image contrast. These new reconstruction algorithms have been proven to improve the SNR and the CNR. A study has confirmed that reconstructed MEI (+) at 40 keV shows the highest CNR for the evaluation of breast cancer (8). However, the study recommends that the 50-keV image series were the most clinically useful for breast cancer detection owing to the relatively low image noise. In our study, the objective image noise characteristics of MEI (+) reconstructions were comparable with those of the latest studies that showed increased noise at lower energy levels (7, 22). Although the image noise was slightly higher at 40 keV MEI (+), we found that the best CNR and SNR for breast lesions were obtained with MEI (+) at 40 keV, and the net benefit of increased tissue contrast seems to exceed the drawbacks.

In recent years, DECT quantitative parameters have been proven useful in evaluating neoangiogenesis and have been increasingly applied in tumor detection and characterization (23). The NIC can reveal an increase in tumor neovascularization, while the λ_{HU} and the nZ_{eff} can provide quantitative information about tissue composition, overcoming the limitations of attenuation-based conventional single-energy CT imaging (24-26). In our study, the NIC, the nZ_{eff}, and the λ_{HU} of malignant breast lesions in the venous phase were higher than those in the arterial phase. It should be noted that our scanning protocol is designed for the thorax, rather than specifically for the breast. The average acquisition times in the arterial and venous phases were 35 ± 5 seconds and 60 ± 7 seconds after injection of contrast media, respectively. Therefore, the venous phase in our study corresponds to the early phase in terms of the MR protocol. According to a previous study (8), the optimal scanning time for the breast is 40–60 seconds during the early phase and 120–180 seconds during the late phase after injection. Results from dynamic contrast-enhanced MRI (27) and contrast-enhanced spectral mammography (28) also suggest taking post-contrast

 https://doi.org/10.3348/kjr.2020.0310

images 2 minutes after the injection of contrast media to increase the conspicuity of malignant lesions. Consistent with the abovementioned, we found that the value of the quantitative parameters of the venous phase was higher than that of the parameters of the arterial phase, but no "wash out" signs were observed. We believe that a tailored contrast enhancement DECT scanning protocol for breast tissue is needed and should be explored in the future.

In the subjective image assessment, the lesion conspicuity score was significantly higher in MEI (+) at 40 keV and in ID and Z_{eff} reconstructions than in PEI, consistent with the results of previous studies (6, 17, 29, 30), which is a consequence of the increased attenuation of iodine at energy levels close to its absorption maximum (33 keV) (31). Similar results can be seen in the color-coded ID and Z_{eff} reconstruction images in our study. This may be related to the fact that the human eye is much more sensitive to color than to grayscale. We hope that color CT imaging can become the future of tumor detection.

Previous studies have concluded that the assessment of morphological and contrasting features of the mass by routine contrast-enhanced thorax CT scans is useful for discriminating between malignant and benign breast lesions (20, 32, 33). A study has shown that 40 keV DECT images can detect intraductal components more accurately than MRI because fine structures are more distinct in 40 keV images (34). Our results show that the mass margins were significantly clearer and that there was more visual enhancement of the lesion in MEI (+) at 40 keV than in PEI. Therefore, we speculate that a morphological analysis with MEI (+) at 40 keV is more conclusive regarding the differentiation between malignant and benign breast lesions, and we hope to verify these findings in future studies.

This study has several limitations. First, it was a retrospective study with a relatively small patient cohort, and tumor sizes smaller than 1 cm were not included. Second, benign breast lesions were excluded. Therefore, we did not distinguish between benign and malignant lesions by using the NIC, the nZ_{eff}, and the λ_{HU}. Third, based on previous research, we only described the visual enhancement as "poor" or "good" rather than as homogeneous/ heterogeneous/ rim enhancement. Finally, our study was primarily based on thorax CT scans; therefore, the appropriate scanning time after contrast media injection to identify breast cancer could not be determined. In future studies, the conspicuity of breast lesions as assessed by dynamic studies with late phase images should be further explored.

In conclusion, This study showed that MEI (+) reconstructions acquired at low keV levels provide improved objective and subjective assessment of lesion conspicuity compared with PEI in patients with breast cancer. Multiple quantitative DECT parameters of malignant breast lesions in the venous phase were higher than those in the arterial phase. MEI (+) reconstruction acquired by DECT may be helpful for the preoperative evaluation of breast cancer.

Conflicts of Interest

The authors have no potential conflicts of interest to disclose.

Acknowledgments

The authors thank all volunteers who participated in the study and the staff of the Department of Radiology, Chongqing University Cancer Hospital & Chongqing Cancer Institute & Chongqing Cancer Hospital in Chongqing, China, for their selfless and valuable assistance.

ORCID iDs

Xiaoxia Wang
https://orcid.org/0000-0002-9540-0677
Daihong Liu
https://orcid.org/0000-0001-5606-4394
Shixi Jiang
https://orcid.org/0000-0002-9737-1689
Xiangfei Zeng
https://orcid.org/0000-0001-7192-6079
Lan Li
https://orcid.org/0000-0002-0038-1953
Tao Yu
https://orcid.org/0000-0002-9618-2755
Jiuquan Zhang
https://orcid.org/0000-0003-0239-6988

REFERENCES

1. Bray F, Ferlay J, Soerjomataram I, Siegel RL, Torre LA, Jemal A. Global cancer statistics 2018: GLOBOCAN estimates of incidence and mortality worldwide for 36 cancers in 185 countries. *CA Cancer J Clin* 2018;68:394-424
2. Shimauchi A, Yamada T, Sato A, Takase K, Usami S, Ishida T, et al. Comparison of MDCT and MRI for evaluating the intraductal component of breast cancer. *AJR Am J Roentgenol* 2006;187:322-329

https://doi.org/10.3348/kjr.2020.0310

3. Brown JC, Kontos D, Schnall MD, Wu S, Schmitz KH. The dose-response effects of aerobic exercise on body composition and breast tissue among women at high risk for breast cancer: a randomized trial. *Cancer Prev Res (Phila)* 2016;9:581-588
4. Casiraghi M, De Pas T, Maisonneuve P, Brambilla D, Ciprandi B, Galetta D, et al. A 10-year single-center experience on 708 lung metastasectomies: the evidence of the "international registry of lung metastases". *J Thorac Oncol* 2011;6:1373-1378
5. Mahner S, Schirrmacher S, Brenner W, Jenicke L, Habermann CR, Avril N, et al. Comparison between positron emission tomography using 2-[fluorine-18]fluoro-2-deoxy-D-glucose, conventional imaging and computed tomography for staging of breast cancer. *Ann Oncol* 2008;19:1249-1254
6. Beer L, Toepker M, Ba-Ssalamah A, Schestak C, Dutschke A, Schindl M, et al. Objective and subjective comparison of virtual monoenergetic vs. polychromatic images in patients with pancreatic ductal adenocarcinoma. *Eur Radiol* 2019;29:3617-3625
7. De Cecco CN, Caruso D, Schoepf UJ, De Santis D, Muscogiuri G, Albrecht MH, et al. A noise-optimized virtual monoenergetic reconstruction algorithm improves the diagnostic accuracy of late hepatic arterial phase dual-energy CT for the detection of hypervascular liver lesions. *Eur Radiol* 2018;28:3393-3404
8. Okada K, Matsuda M, Tsuda T, Kido T, Murata A, Nishiyama H, et al. Dual-energy computed tomography for evaluation of breast cancer: value of virtual monoenergetic images reconstructed with a noise-reduced monoenergetic reconstruction algorithm. *Jpn J Radiol* 2020;38:154-164
9. Metin Y, Metin NO, Özdemir O, Taşçı F, Kul S. The role of low keV virtual monochromatic imaging in increasing the conspicuity of primary breast cancer in dual-energy spectral thoracic CT examination for staging purposes. *Acta Radiol* 2020;61:168-174
10. Patino M, Prochowski A, Agrawal MD, Simeone FJ, Gupta R, Hahn PF, et al. Material separation using dual-energy CT: current and emerging applications. *Radiographics* 2016;36:1087-1105
11. Rassouli N, Etesami M, Dhanantwari A, Rajiah P. Detector-based spectral CT with a novel dual-layer technology: principles and applications. *Insights Imaging* 2017;8:589-598
12. Xu X, Sui X, Zhong W, Xu Y, Wang Z, Jiang J, et al. Clinical utility of quantitative dual-energy CT iodine maps and CT morphological features in distinguishing small-cell from non-small-cell lung cancer. *Clin Radiol* 2019;74:268-277
13. Yang Y, Li K, Sun D, Yu J, Cai Z, Cao Y, et al. Invasive pulmonary adenocarcinomas versus preinvasive lesions appearing as pure ground-glass nodules: differentiation using enhanced dual-source dual-energy CT. *AJR Am J Roentgenol* 2019;213:W114-W122
14. Fehrenbach U, Feldhaus F, Kahn J, Böning G, Maurer MH, Renz D, et al. Tumour response in non-small-cell lung cancer patients treated with chemoradiotherapy - Can spectral CT predict recurrence? *J Med Imaging Radiat Oncol* 2019;63:641-649
15. Goldhirsch A, Winer EP, Coates AS, Gelber RD, Piccart-Gebhart M, Thürlimann B, et al. Personalizing the treatment of women with early breast cancer: highlights of the St Gallen International Expert Consensus on the Primary Therapy of Early Breast Cancer 2013. *Ann Oncol* 2013;24:2206-2223
16. Tashima R, Nishimura R, Osako T, Nishiyama Y, Okumura Y, Nakano M, et al. Evaluation of an optimal cut-off point for the Ki-67 index as a prognostic factor in primary breast cancer: a retrospective study. *PLoS One* 2015;10:e0119565
17. El Kayal N, Lennartz S, Ekdawi S, Holz J, Slebocki K, Haneder S, et al. Value of spectral detector computed tomography for assessment of pancreatic lesions. *Eur J Radiol* 2019;118:215-222
18. Lennartz S, Laukamp KR, Neuhaus V, Große Hokamp N, Le Blanc M, Maus V, et al. Dual-layer detector CT of the head: initial experience in visualization of intracranial hemorrhage and hypodense brain lesions using virtual monoenergetic images. *Eur J Radiol* 2018;108:177-183
19. Zhang X, Zheng C, Yang Z, Cheng Z, Deng H, Chen M, et al. Axillary sentinel lymph nodes in breast cancer: quantitative evaluation at dual-energy CT. *Radiology* 2018;289:337-346
20. Lin YP, Hsu HH, Ko KH, Chu CM, Chou YC, Chang WC, et al. Differentiation of malignant and benign incidental breast lesions detected by chest multidetector-row computed tomography: added value of quantitative enhancement analysis. *PLoS One* 2016;11:e0154569
21. Spak DA, Plaxco JS, Santiago L, Dryden MJ, Dogan BE. BI-RADS® fifth edition: a summary of changes. *Diagn Interv Imaging* 2017;98:179-190
22. Bellini D, Gupta S, Ramirez-Giraldo JC, Fu W, Stinnett SS, Patel B, et al. Use of a noise optimized monoenergetic algorithm for patient-size independent selection of an optimal energy level during dual-energy CT of the pancreas. *J Comput Assist Tomogr* 2017;41:39-47
23. Simons D, Kachelriess M, Schlemmer HP. Recent developments of dual-energy CT in oncology. *Eur Radiol* 2014;24:930-939
24. Johnson TR, Krauss B, Sedlmair M, Grasruck M, Bruder H, Morhard D, et al. Material differentiation by dual energy CT: initial experience. *Eur Radiol* 2007;17:1510-1517
25. Marin D, Boll DT, Mileto A, Nelson RC. State of the art: dual-energy CT of the abdomen. *Radiology* 2014;271:327-342
26. Cai W, Kim SH, Lee JG, Yoshida H. Informatics in radiology: dual-energy electronic cleansing for fecal-tagging CT colonography. *Radiographics* 2013;33:891-912
27. Nunes LW, Englander SA, Charafeddine R, Schnall MD. Optimal post-contrast timing of breast MR image acquisition for architectural feature analysis. *J Magn Reson Imaging* 2002;16:42-50
28. Bhimani C, Matta D, Roth RG, Liao L, Tinney E, Brill K, et al. Contrast-enhanced spectral mammography: technique, indications, and clinical applications. *Acad Radiol* 2017;24:84-88
29. Zopfs D, Laukamp KR, Pinto Dos Santos D, Sokolowski

M, Große Hokamp N, Maintz D, et al. Low-keV virtual monoenergetic imaging reconstructions of excretory phase spectral dual-energy CT in patients with urothelial carcinoma: a feasibility study. *Eur J Radiol* 2019;116:135-143
30. Okada K, Matsuda M, Tsuda T, Kido T, Murata A, Nishiyama H, et al. Dual-energy computed tomography for evaluation of breast cancer: value of virtual monoenergetic images reconstructed with a noise-reduced monoenergetic reconstruction algorithm. *Jpn J Radiol* 2020;38:154-164
31. McCollough CH, Leng S, Yu L, Fletcher JG. Dual- and multi-energy CT: principles, technical approaches, and clinical applications. *Radiology* 2015;276:637-653
32. Lin WC, Hsu HH, Li CS, Yu JC, Hsu GC, Yu CP, et al. Incidentally detected enhancing breast lesions on chest computed tomography. *Korean J Radiol* 2011;12:44-51
33. Moyle P, Sonoda L, Britton P, Sinnatamby R. Incidental breast lesions detected on CT: what is their significance? *Br J Radiol* 2010;83:233-240
34. Yao Y, Nagasawa A, Kakegawa A, Kato M, Kaisaki S, Sakatani T. An attempt to evaluate intraductal components of breast cancer by dual energy computed tomography. *Imaging Med* 2018;10:103-110

https://doi.org/10.3348/kjr.2020.0310